

1 A bias-corrected & downscaled massive ensemble to diagnose  
2 uncertainty in climate impact projections

3 Kevin Schwarzwald <sup>\*1,2</sup>, Nathan Lenssen<sup>3,4</sup>, Radley M. Horton<sup>1,2</sup>, and Gernot Wagner<sup>5</sup>

4 <sup>1</sup>Columbia Climate School, New York, NY, USA

5 <sup>2</sup>Lamont-Doherty Earth Observatory of Columbia University, Palisades, NY, USA

6 <sup>3</sup>Colorado School of Mines, Golden, CO, USA

7 <sup>4</sup>NSF National Center for Atmospheric Research, Boulder, CO, USA

8 <sup>5</sup>Columbia Business School, New York, NY, USA

9 **Abstract**

10 Projections of climate change and climate impacts requires bias-corrected, downscaled output from  
11 ensembles of earth system models (ESMs). Potential impacts are uncertain due to modeling differences  
12 between ESMs, internal variability stemming from the chaos of the earth system, and differences in the  
13 historical reference datasets used to bias-corrected and downscale ESM output. Here, we introduce the  
14 Bias-Corrected and Downscaled Massive Ensemble (BCD-ME), a set of over 1,400 projections of daily  
15 mean and maximum temperature. The BCD-ME samples model and internal uncertainty with up to 86  
16 runs from 12 Large Ensembles and uncertainty in the reference dataset by using 4 different reanalysis  
17 products to bias-correct and downscale output. Output is organized by Global Warming Levels (GWL),  
18 accounting for differences between forcing scenarios and ESM climate sensitivities. The ensemble contains  
19 20-year daily time series for each GWL on a uniform 1° grid, bias-corrected using Quantile Delta Mapping,  
20 and statistics of 20-year time series for each GWL on a uniform 0.25° grid, downscaled using Quantile-  
21 Preserving Localized Analog Downscaling. The BCD-ME is stored in Analysis-Ready, Cloud-Optimized  
22 (ARCO) Zarr stores, enabling efficient computation of the 97 TB (uncompressed) dataset.

---

\*Correspondence to kevin.schwarzwald@columbia.edu

# 1 Background & Summary

Climate impact assessments help predict changes in human and natural systems due to climate change. Generally, these studies seek to find a statistical or process-based relationship between the climate and an impact over some observed, historical period and then use this relationship to predict changes in the impact given some change to the climate. Estimates of future climates are critical in this process, generally referred to as “climate projections”. Climate projections are most commonly derived from simulations made with dynamical Earth System Models (ESMs) as part of the Coupled Model Intercomparison Project (CMIP)<sup>1</sup>.

There are three major knowledge barriers to properly using CMIP-class ESMs’ climate projections in climate impacts studies. First, uncertainty in future climate must be included and properly propagated to the estimate of future impacts, stemming from differences between forcing scenarios, differences between ESMs, and the internal variability due to the chaotic nature of the earth system<sup>2-6</sup>. The climate impacts community is increasingly accounting for climate uncertainty due to possible future scenarios and differences in climate models<sup>7</sup>. Including uncertainty due to internal climate variability has been shown to be important as well, but has lagged, since proper treatment of internal uncertainty requires applying analyses to hundreds of climate model projections<sup>6</sup>.

Second, raw values from ESM output are biased relative to the true Earth’s climate in both the mean and higher moments of key climate variables. While ESMs simulate the climate with underlying physics, chemistry, and biology as currently understood, due to modeling limitations they do not exactly replicate the observed climate, and are run with no requirement that the output has equal statistics to the true Earth system<sup>4;8</sup>; ESM output must, thus, be bias-corrected before it can be used in impacts contexts<sup>4</sup>.

Finally, CMIP-class ESMs generally utilize atmospheric models with spatial resolutions of 0.7 – 2.8° (approx. 100-300 km at the equator) and are therefore unable to provide local estimates of key variables at impact-relevant spatial scales, particularly in regions with complex geography<sup>9;10</sup>; ESM output is, thus, often downscaled before use in impacts contexts.

Bias-correction and statistical downscaling methods require a spatially and temporally complete product of observed climate. Climate reanalyses or other gridded historical data products are typically used for this purpose as direct weather observations have gaps in spatial and temporal coverage, particularly prior to the satellite era. However, reanalyses provide imperfect estimates of climate variables with uncertainty arising due to limitations in the dynamical model, the assimilation scheme, and uncertainty in the data assimilated into the reanalysis, adding an additional source of uncertainty in climate projections.

To properly overcome all three of these knowledge barriers, a research group must therefore have sufficient computational resources and technical expertise to download and store hundreds of climate model projections,

55 implement or develop bias-correction and downscaling methods, and apply these to each climate projection.  
56 Together, these steps are a massive investment in computing, disk storage, and software development that  
57 all ought to be supported by expertise from climate and statistical experts. The scale of this investment  
58 is a major barrier to entry into studying climate impacts. Existing publicly-available products aimed at  
59 impacts research, such as NASA Earth Exchange Global Daily Downscaled Projections (NEX-GDDP)<sup>11</sup>,  
60 the Inter-Sectoral Impact Model Intercomparison Project (ISIMIP)<sup>12</sup>, or the Global Downscaled Projections  
61 for Climate Impact Research (GDPCIR)<sup>13</sup> provide bias-corrected and downscaled climate projections, but  
62 do not sample internal variability (only one ensemble member per ESM is provided). A notable exception  
63 are the recent GARD-LENS<sup>14</sup> and LOCA2<sup>15</sup> products, which provide output from several large ensembles  
64 at very high resolution; however, these products are limited to North America. Furthermore, none of these  
65 products samples the uncertainty in datasets used to post-process ESM output (only one reanalysis or other  
66 gridded historical reference dataset is used in each product).

## 67 1.1 Summary of the BCD-ME

68 To fill this gap, in this data descriptor we present the Bias-Corrected & Downscaled Massive Ensemble (BCD-  
69 ME), a near-surface air temperature projection dataset designed to make it as straightforward as possible  
70 to include climate uncertainty in analyses. The BCD-ME addresses the knowledge barriers discussed above,  
71 including uncertainty due to the reanalysis product used. The key features of this dataset include:

- 72 • **Daily average and maximum temperature with near-global land coverage** to enable global  
73 and regional analyses of temperature projections and climate impact projections.
- 74 • **Indexed by global warming levels (GWLs)** to facilitate direct comparisons of ESMs with different  
75 climate sensitivities.
- 76 • **Bias-Corrected** time series on a uniform 1° grid using Quantile Delta Mapping (QDM)<sup>16</sup>.
- 77 • **Downscaled** statistics of bias-corrected time series on a 0.25° grid using Quantile-Preserving Localized  
78 Analog Downscaling (QPLAD)<sup>13</sup>.
- 79 • **Sampling climate model uncertainty** using 12 different ESMs
- 80 • **Sampling internal variability** using between 5 and 86 ensemble members from each ESM.
- 81 • **Sampling “ground-truth” uncertainty** using 4 reanalyses of historical climate to bias-correct and  
82 downscale ESM output.
- 83 • **Provided in Zarr stores** and on the cloud for efficient computation.

84 We use four products as possible observational ground truths in the bias-correction and downscaling.  
85 (1) The European Centre for Medium-Range Weather Forecasting Reanalysis v5 (ERA5)<sup>17</sup> (2) The NASA  
86 Modern-Era Retrospective analysis for Research and Applications, Version 2 (MERRA2)<sup>18</sup> (3) The Japanese  
87 Meteorological Agency Japanese Reanalysis for Three Quarters of a Century (JRA-3Q)<sup>19</sup> (4) The Global Me-  
88 teorological Forcing Dataset (GMFD)<sup>20</sup>. The first three are state-of-the-art operational reanalyses. GMFD  
89 is included as it is used to bias-correct the NASA NEX-GDDP<sup>11</sup> and is therefore commonly used in climate  
90 impact research<sup>21–23</sup>.

91 The BCD-ME contains two collections of data: (1) bias-corrected time series on a uniform  $1^\circ \times 1^\circ$  grid  
92 and (2) selected metrics commonly used in climate impacts studies on a uniform  $0.25^\circ \times 0.25^\circ$  (see Table 3  
93 for descriptions). We provide statistics on the downscaled  $0.25^\circ$  grid, rather than the full daily time series, to  
94 increase the usability of this very large dataset. The BCD-ME time series collection provides bias-corrected  
95 time series 2m daily temperature (`tas`) and 2m maximum daily temperature (`tasmax`) for all locations from  
96  $56^\circ\text{S}$  to  $86^\circ\text{N}$  (land-only for GMFD-based ensemble members), spanning all permanently inhabited regions.  
97 The  $0.25^\circ$  downscaled product provides bias-corrected and downscaled metrics for all land locations over the  
98 same spatial extent.

99 The presented BCD-ME dataset contains on the order of 100 times more impact assessment-ready temper-  
100 ature projections than the commonly used NASA NEX-GDDP dataset<sup>11</sup>. The organization of the BCD-ME  
101 enables users to easily account for all sources of climate uncertainty by indexing across uncertainty-relevant  
102 dimensions. The computational costs of scaling an impacts analysis by a factor of 100 is reduced by providing  
103 the BCD-ME as I/O-optimized Zarr stores that enable code bases to be easily scaled and parallelized on  
104 modest systems.

105 In the remainder of this paper, we outline the source data and methods used to construct the BCD-ME,  
106 provide a validation of the dataset, and provide suggestions for best practices when working with this data.  
107 We expect that the BCD-ME will be useful for users of climate projection information by enabling the robust  
108 quantification of uncertainty in future climate.

## 109 2 Methods

110 There are four major components in the creation of the BCD-ME (see summary diagram in Figure 1). Section  
111 2.1 details the ESM and reanalysis data used as the raw inputs to the BCD-ME. Section 2.2 discusses how  
112 GWLs are calculated for each climate projection, how the data is organized by these GWLs, and presents  
113 analysis justifying the use of GWLs. Section 2.3 details the bias-correction methods and Section 2.4 details  
114 the downscaling method.

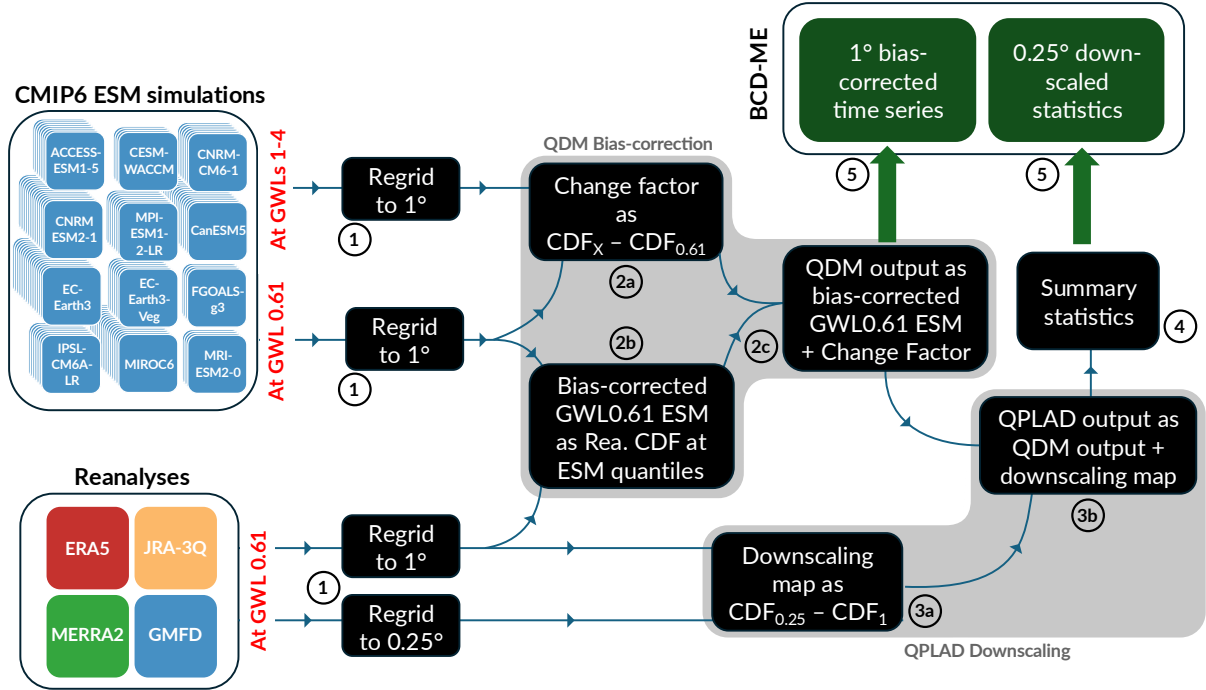


Figure 1: Diagram of bias-correcting and downscaling workflow. Reanalysis data for the 20 years around GWL0.61 (1982-2001) is regrided to uniform 1° and 0.25° grids; data from ESM runs for the 20 years around GWLs 0.61 and 0.5°C steps from GWL1 to 4 (or the highest GWL step reached) are regrided to a uniform 1° grid (Step 1). Processing is done separately for each combination of an ESM run and a reanalysis ‘ground truth’. 1-degree ESM and reanalysis data is used to create bias-corrected time series through the QDM methodology (Step 2). That bias-corrected output is combined with a downscaling map from reanalysis between 1° and 0.25° to create downscaled time series through the QPLAD methodology (Step 3). Finally, summary statistics (detailed in Table 3) of the 0.25°-degree time series are calculated (Step 4). For each ESM run and reanalysis, one set of bias-corrected time series on a 1° grid and one set of statistics of the bias-corrected and downscaled time series on a 0.25° grid are thus saved, forming the BCD-ME (Step 5).

## 115 2.1 Input Data

### 116 2.1.1 CMIP6 Large Ensemble MIP

117 We aim to use all simulations from the CMIP6 Large Ensemble MIP available on Pangeo’s CMIP6 cloud stor-  
 118 age (<https://console.cloud.google.com/marketplace/product/noaa-public/cmip6>) that have daily  
 119 output for daily mean (`tas`) or max (`tasmax`) near-surface air temperature for a historical experiment  
 120 starting at the latest on January 1, 1850, and a future ScenarioMIP experiment forced with any Shared  
 121 Socioeconomic Pathway (SSP)<sup>24</sup>, resulting in 12 ESMs with ensemble sizes ranging from 8 to 86. Currently,  
 122 this includes 365 total members for `tas` and 190 for `tasmax`, with future versions of the dataset including  
 123 more members as they are processed or become available on pangeo. These ensemble sizes include all pro-  
 124 jections run with the model, across all SSPs. A full description of the ESMs used is shown in Table 4. Note  
 125 that ESM output is regrided bilinearly to a uniform 1-degree latitude/longitude grid before bias-correction

Reanalysis	Resolution	Publisher	Citation
ERA5	0.25°	European Centre for Medium-Range Weather Forecasting (ECMWF)	17
MERRA2	0.5° x 0.625°	National Aeronautics and Space Administration (NASA)	25
JRA-3Q	0.375°	Japan Meteorological Agency (JMA)	19
GMFD	0.25 °	Princeton Hydrology Group	20

Table 1: Reanalysis products used as historical “ground truths” for bias-correction and downscaling

126 (Step 1 in Figure 1).

### 127 2.1.2 Global Reanalysis

128 Bias-correction and downscaling both rely on knowing the Earth’s true climate over some observed time  
129 period. However, there is non-negligible uncertainty in estimates of the true historical climate<sup>26;27</sup>. Despite  
130 this uncertainty, climate impact studies generally use a single reanalysis product, failing to sample both  
131 uncertainty in the raw data assimilated into the reanalysis as well as structural uncertainties in the underlying  
132 dynamical model. In the BCD-ME, we sample this reanalysis uncertainty by repeating the bias-correction and  
133 downscaling with four reanalyses (see Table 1): the European Centre for Medium-Range Weather Forecasting  
134 ERA5<sup>17</sup>, NASA MERRA2<sup>25</sup>, the Japan Meteorological Agency JRA-3Q<sup>19</sup>, and GMFD<sup>20</sup>. ERA5, MERRA2,  
135 and JRA-3Q are latest-generation, continuously updating global reanalysis products, while GMFD is used  
136 as the “ground truth” for NASA’s NEX GDDP<sup>11</sup> set of bias-corrected and downscaled climate projections  
137 and is therefore frequently used as a source of historical weather observations in projections of climate  
138 impacts<sup>21–23</sup>. While this is not a complete assessment of uncertainty in the observed climate, there are  
139 substantial differences between these four products, providing the ability to determine the sensitivity of  
140 climate impact projections to the choice of ground-truth observations.

141 Reanalysis products are used at two resolutions (Step 1 in Figure 1). For bias-correction, output from  
142 reanalyses is bilinearly regridded to a uniform 1-degree latitude/longitude grid. For downscaling, output  
143 from reanalyses is bilinearly regridded to a uniform 0.25-degree latitude/longitude grid that exactly nests  
144 into the 1-degree grid such that each 1-degree grid cell contains 4 0.25-degree grid cells.

145 Note that 0.25 degree is a finer resolution than two of the reanalyses used (MERRA2 and JRA-3Q). Thus,  
146 the 0.25 degree projections from MERRA2 and JRA-3Q cannot contain information finer than the native  
147 grids of these reanalyses (See Table 1) and are constructed by interpolation from these native reanalysis  
148 grids. Nevertheless, we provide all four downscaled products at the 0.25 degree grid to facilitate comparison.  
149 Users should use caution when interpreting fine-scale spatial features in MERRA2 and JRA-3Q 0.25 degree  
150 projections.

## 151 2.2 Global Warming Levels

152 Rather than providing projections as continuous time series over the 21st century, we instead organize the  
153 BCD-ME by 20-year daily time series at given Global Warming Levels (GWLs). GWLs are degrees of global  
154 mean near-surface air temperature warming relative to the 1850-1900 baseline<sup>28</sup>. For instance, the ‘2°C  
155 world’ envisioned by the Paris Agreement considers climate conditions and impacts at GWL2.

156 Future climate impacts are increasingly presented by GWL including in the sixth IPCC assessment  
157 report, due to several key advantages over time-series-based projections. First, data presented at GWLs is  
158 agnostic to climate sensitivity, helping avoid the so called “hot model” problem from ESMs with possibly  
159 unrealistically high climate sensitivities in CMIP6<sup>29</sup>. Note that this removes intermodel differences in global  
160 climate sensitivity as a driver of model uncertainty; the intermodel spread will therefore be reduced compared  
161 to an analysis at a comparative set of calendar years.

162 Second, data presented at GWLs control for differences between climate scenarios, such as the Shared  
163 Socioeconomic Pathways (SSPs)<sup>24</sup> used in the CMIP6 ScenarioMIP set of experiments. These SSPs are  
164 socioeconomic storylines of future anthropogenic forcings, such as greenhouse gas and aerosol concentrations  
165 or land use patterns, and are not intended to provide a statistical sampling of plausible future conditions.  
166 Abstracting away from differences in warming rates between SSPs allows a user to assume their own pre-  
167 ferred timeline of warming (including by examining scenarios such as the Paris Agreement or using GMSTs  
168 estimated from integrated assessment models).

169 Third, by pooling ensemble members from different SSPs at the same GWL, users of climate data are  
170 able to boost the ensemble size for each ESM. These larger ensemble sizes enable characterization of ESM  
171 internal variability for a larger set of ESMs<sup>30</sup>.

### 172 2.2.1 GWL Identification and Data Organization

173 In the BCD-ME, we utilize a global warming level index **GWL** rather than indexing by a calendar year in the  
174 future, providing 20 years of daily simulations at 8 GWLs: 0.61, 1.0, 1.5, 2.0, 2.5, 3.0, 3.5, and 4.0 °C. The  
175 0.61 °C equals the observed global mean temperature over the 20 year period of 1982-2001 in HadCRUT5<sup>26</sup>  
176 and was used as a reference time to bias-correct and downscale ESM output, and together with GWL1  
177 (2001-2020 in HadCRUT5) may be useful for climate impact studies that investigate the changes in climate  
178 risk compared to a period close to present.

179 A GWL is defined by the global mean temperature anomaly relative to a 1850-1900 baseline following  
180 the IPCC definition for warming compared to the preindustrial. For each climate model ensemble member,  
181 we calculate the global mean surface annual temperature anomaly and compute a 20 year moving average.

Variable	GWL reached: Model	1.0	1.5	2.0	2.5	3.0	3.5	4.0
tas	ACCESS-ESM1-5	24	24	24	24	5	5	5
	CESM2-WACCM	8	8	8	7	7	4	3
	CNRM-CM6-1	18	18	18	18	15	12	6
	CNRM-ESM2-1	41	41	31	26	13	7	5
	CanESM5	86	86	86	86	86	86	79
	EC-Earth3	35	35	35	35	32	15	10
	EC-Earth3-Veg	13	13	13	13	13	9	6
	FGOALS-g3	10	10	10	7	3	0	0
	IPSL-CM6A-LR	28	28	28	28	28	18	17
	MIROC6	60	34	34	31	28	0	0
	MPI-ESM1-2-LR	30	30	30	20	16	6	0
MRI-ESM2-0	12	8	8	8	7	2	0	
	Total	365	335	325	303	253	164	131
tasmax	ACCESS-ESM1-5	6	6	6	6	6	6	6
	CESM2-WACCM	0	0	0	0	0	0	0
	CNRM-CM6-1	5	5	5	3	2	2	1
	CNRM-ESM2-1	5	5	3	3	2	1	1
	CanESM5	30	30	30	30	30	30	27
	EC-Earth3	22	22	22	22	19	8	3
	EC-Earth3-Veg	10	10	10	10	10	5	2
	FGOALS-g3	7	7	7	4	0	0	0
	IPSL-CM6A-LR	22	22	22	22	22	12	11
	MIROC6	37	25	25	22	19	0	0
	MPI-ESM1-2-LR	30	30	30	20	16	6	0
MRI-ESM2-0	16	16	16	14	11	6	0	
	Total	190	178	176	156	137	76	51

Table 2: Number of runs in the BCD-ME that (as of version 1) have data for at least a given GWL, by ESM, for near-surface mean daily air temperature (`tas`, top half) and near-surface maximum daily air temperature (`tasmax`, bottom half).

182 Then, for each GWL, we find the first year that this moving average crosses the given GWL, and define the  
183 20 years around this year as the climate for this GWL<sup>28;31</sup>.

184 For a given GWL, 20 years of daily temperature fields are then provided in the BCD-ME, indexed by  
185 `year` from 1:20 and `dayofyear` from 1:365. As an example, in the `r1i1p1f1` member of the MPI-ESM1-LR  
186 model run under SSP2.45, the 20-year rolling average of global mean temperature is more than 1 degree  
187 above its 1850-1900 mean for the first time in 2013. Thus, we define the 20-year time period of 2003-2022 as  
188 an ensemble member for this model for the 1.0 °C GWL. We additionally provide the calendar years from  
189 the ESM simulation as the auxiliary dimension `calendar_year`, but recommend users utilize the GWL setup  
190 of the data whenever possible. Note that many model projections will not reach every GWL, with only  
191 the warmest models under high emissions scenarios reaching the 4.0 °C GWL. The number of simulations  
192 available at each GWL for each model is presented in Table 2.

### 2.3 Bias-Correction: Quantile Delta Mapping

Since the probability distributions of climate variables in an ESM differ from those in the true Earth, ESM output is generally bias-corrected in climate impacts context to make values directly usable in climate impact models trained on historical observations.

Here, we use the Quantile Delta Mapping (QDM)<sup>16</sup> method (Step **2** in Figure 1). QDM uses a “delta method” approach, adding changes between present and future time periods from an ESM to a time series taken from a reference data product. QDM allows for different change factors for each quantile of an ESM’s distribution. That change factor is then added to the reference data sampled at the quantiles of the ESM’s time series, equivalently referred to as a bias-corrected version of the historical ESM data<sup>16</sup>.

Each day-of-year is processed separately using a moving window of 31 days for each day-of-year to calculate CDFs. At a given location and each day of year, the changes between the empirical CDF of the ESM run at a reference GWL (0.61, representing 1982-2001 in the real world) and the empirical CDF of a future GWL is found, using 100 samples of quantiles to estimate the CDF (Step **2a**). Then, for each day in the future period, the same quantile is found in the reference reanalysis dataset (Step **2b**), and the difference in the CDF at that quantile and day of year of the GWL is added to it (Step **2c**). The difference between the future ESM and GWL 0.61 ESM CDFs thus provides the necessary correction factor of the reanalysis data. That is, for  $x_m(t)$ , a ESM projection  $m$  at time  $t$  in the future, we calculate the adjusted  $x_m^*(t)$  as:

$$x_m^*(t) = x_m(t) + (F_o^{-1}(q) - F_m^{-1}(q)) \quad (1)$$

where  $F_o^{-1}$  and  $F_m^{-1}$  are the empirical inverse CDFs of the observed historical climate and the ESM climate respectively. Finally,  $q$  is the quantile associated with the value of  $x_m(t)$  in the ESM’s simulation. We roughly follow the notation in Section 3.1 of Gergel et al. (2024)<sup>13</sup> which contains more background on this method.

As an example, if the 0.6 quantile of a ESM simulation at a location at GWL1 is 14.5 °C and the 0.6 quantile of the same ESM run at this same location at GWL0.61 is 13.8 °C, the 0.6 quantile from the reanalysis for this day of year is projected by adding 0.7 °C.

### 2.4 Downscaling: Quantile-Preserving Localized-Analog Downscaling

The Large Ensemble ESMs simulation used here for temperature projections have native grids ranging in resolution from 0.7° to 2.8° (approx. 100-300 km at the equator). There is need in the climate impact community for information at as fine a spatial scale as possible, motivating the downscaling of these products.

221 Here, we implement Quantile-Preserving Localized-Analog Downscaling (QPLAD) for statistically downscal-  
222 ing the ESM output to a finer resolution reanalysis grid, following Gergel et al. (2024)<sup>13</sup> (Step **3** in Figure  
223 1).

224 Similar to the QDM bias-correction, QPLAD is a non-parametric quantile-based method that provides  
225 estimates of the temperature at the fine-scale. First, a downscaling map is created using the reference  
226 reanalysis datasets (Step **3a** in Figure 1). We use the 1982-2001 reanalysis data regridded to a 1-degree grid  
227 from above, and also bilinearly regrid the reanalysis data to a uniform 0.25-degree grid that perfectly slots  
228 into the 1-degree grid such that each low-resolution grid cell exactly contains 4 high-resolution grid cells.  
229 For each reanalysis, the downscaling map is the difference in empirical CDFs (using all empirical quantiles)  
230 between the 1-degree data and the 0.25-degree data. As before, separate CDFs are calculated for each day-  
231 of-year, using a 31-day rolling window across each of the 20 years centered at that day-of-year, resulting in  
232 620 (31 x 20) empirical quantiles.

233 Then, for each day at every location and GWL in each 1-degree bias-corrected ESM simulation, the  
234 downscaling map at the relevant day-of-year and quantile (as before, calculated relative to a 31-day-of-year  
235 moving window across years) is added to its value to produce values at each of the 4 nested 0.25-degree grid  
236 cells within (Step **3b** in Figure 1). See Gergel et al. (2024)<sup>13</sup> for more details.

237 We note that, of the four reanalysis datasets used as downscaling “ground truths”, JRA-3Q (0.375°) and  
238 MERRA2 (0.5° x 0.675°) are of lower resolution than the 0.25-degree resolution of the downscaled datasets.  
239 We use them to downscale to the same uniform 0.25-degree grid as reference, but note that values of the  
240 downscaling map at a higher resolution than their native resolution are statistically interpolated and do not  
241 provide more information from the model. Users should therefore treat those values with caution.

#### 242 **2.4.1 Downscaled metrics**

243 Due to the size of the dataset, we do not provide full time series at the 0.25-degree resolution of the downscaled  
244 data. Rather, we save summary statistics commonly-used in climate impacts work, averaged across the 20  
245 years for each GWL (Step **4** in Figure 1; see Table 3 for details).

246 For both mean and maximum daily temperature, we save the number of days in 1 °C and 5 °F bins  
247 (`tasbinC`, `tasbinF`, `tasmaxbinC`, and `tasmaxbinF`). These are commonly used in binned non-parametric  
248 statistical impact models and to study threshold exceedance following Schlenker et al. (2009)<sup>32</sup> and Deschênes  
249 and Greenstone (2011)<sup>33</sup>. We also provide summed polynomials up to degree 4, allowing for flexible nonlinear  
250 dose-response functions (see, e.g., Carleton et al. (2022)<sup>21</sup>), as `tassumpoly` and `tasmaxumpoly`:

Metric	Units	Description	Notes
<i>Bias-corrected variables (1° grid)</i>			
<code>tas</code>	K	Near-surface mean daily temperature	Time series
<code>tasmax</code>	K	Near-surface maximum daily temperature	Time series
<i>Bias-corrected and downscaled metrics (0.25° grid)</i>			
<code>tasbinC</code>	days / year	Mean days per year in Celsius bins	1-deg bins from -21.5 to 51.5°C
<code>tasbinF</code>	days / year	Mean days per year in Fahrenheit bins	5-deg bins from -5 to 130 F
<code>tassumpoly</code>	°C <sup>k</sup> for $k \in (1, 2, 3, 4)$	Mean annual sums of polynomial mean temperature	
<code>tasmaxbinC</code>	days / year	Mean days per year in Celsius bins	1-deg bins from -21.5 to 51.5°C
<code>tasmaxbinF</code>	days / year	Mean days per year in Fahrenheit bins	5-deg bins from -5 to 130 F
<code>tasmaxsumpoly</code>	°C <sup>k</sup> for $k \in (1, 2, 3, 4)$	Mean annual sums of polynomial max temperature	

Table 3: Description of saved variables in the 1° bias-corrected and 0.25° bias-corrected and downscaled BCD-ME products.

$$sumpoly = \sum_{d=1}^{365} T^k \text{ for } k \in \{1, 2, 3, 4\}$$

251 In other words,  $k = 2$  shows the sum of squared temperature.

### 252 3 Data Records

253 The BCD-ME is presented as an ensemble with multiple ESMs and multiple ensemble members from each  
254 of the ESMs. Rather than providing the full daily time series over the projection period of 2015-2100, we  
255 instead provide 20-year daily time series (for the 1-degree bias-corrected set) and statistics of 20-year daily  
256 time series (for the downscaled 0.25-degree set) from each ESM such that the ESM ensemble mean has a  
257 specific global mean temperature value or global warming level (GWL). There has been a recent shift to  
258 using GWLs instead of time periods in climate projection-related studies, primarily due to the fact that the  
259 CMIP6 generation contains models with climate sensitivities outside the range deemed to be plausible or  
260 the so-called “hot model” problem<sup>29</sup>). Thus, we provide 20-year series at 0.61 °C (equivalent to the mean  
261 observed global temperature from 1982-2001 in HadCRUT5<sup>26</sup>) of warming relative to 1850-1900 (historical)  
262 as well as GWLs of 1.0-4.0 °C in 0.5 °C increments. Thus, including the four different reanalyses used in  
263 bias-correction and the GWLs, the dataset can be viewed as a 7-dimensional array

$$\text{BCD-ME}[\text{lon, lat, time, GWL, reanalysis, ESM, experiment/ensemble\_member}] \quad (2)$$

264 for the 1-degree time series and

$$\text{BCD-ME}[\text{lon, lat, D, GWL, reanalysis, ESM, experiment/ensemble\_member}] \quad (3)$$

265 for the 0.25-degree statistics, with the dimension D being unique to each particular variable (e.g., temperature  
266 bin).

267 To facilitate computation with this massive array, all of the data has been archived in the `Zarr` format,  
268 with a separate `Zarr` store for each ESM and data type. For example, for the ESM ACCESS-ESM1-5, one  
269 `Zarr` store contains all 1° bias-corrected time series in variables `tas` and `tasmax`, and one `Zarr` store contains  
270 all 0.25° downscaled statistics from both `tas`-based and `tasmax`-based variables. We recommend working  
271 with the data in Python with the `Xarray` and `Dask` libraries as these packages make parallelized I/O and  
272 computation relatively simple and efficient to implement<sup>34</sup>.

273 The `Zarr` stores are chunked to facilitate regional analyses. In other words, a chunk will contain all  
274 days (for bias-corrected time series) or all bins or polynomial degrees (for downscaled statistics) for a sub-  
275 continental-scale region for one ensemble member, GWL, and reanalysis.

276 Since not every ensemble member reaches every GWL, and not every ensemble member has data for each  
277 variable, each `Zarr` store contains a metadata coordinate `has_data`, a `variable x ensemble member x GWL`  
278 boolean array detailing which elements have data.

279 The full BCD-ME data is stored and hosted as `Zarr` stores in two repositories: one that will be frozen  
280 upon the publication of this article and one that will be updated. The dataset (in its form upon acceptance of  
281 this manuscript) will be archived in the National Science Foundation (NSF) National Center for Atmospheric  
282 Research (NCAR)’s Geoscience Data Exchange (GEX). The NSF NCAR GEX provides open access to data  
283 through HTTPS and Globus, promotes FAIR principles including issuing a DOI, and enables users to work  
284 quickly with the data on the NCAR computer systems.

285 The BCD-ME is also hosted as `Zarr` stores in the Arraylake cloud storage system in the Earthmover  
286 Marketplace using the Icechunk storage engine in the `s3://ems-climate-uncertainty-lab` bucket. This  
287 version of the BCD-ME is a “cloud-native data repository”<sup>34</sup> that allows fast and efficient processing despite  
288 its size, with access occurring natively within `xarray`. Links to sample code to access this data is provided  
289 in the Data Availability section below. The version of this dataset will not be frozen, but any updates to the  
290 data will be fully tracked through version control, similar to how code revisions are documented through git  
291 repositories. Users accessing this repository will have the latest version of this data and improved I/O due  
292 to the optimizations of handling array data provided by Icechunk.

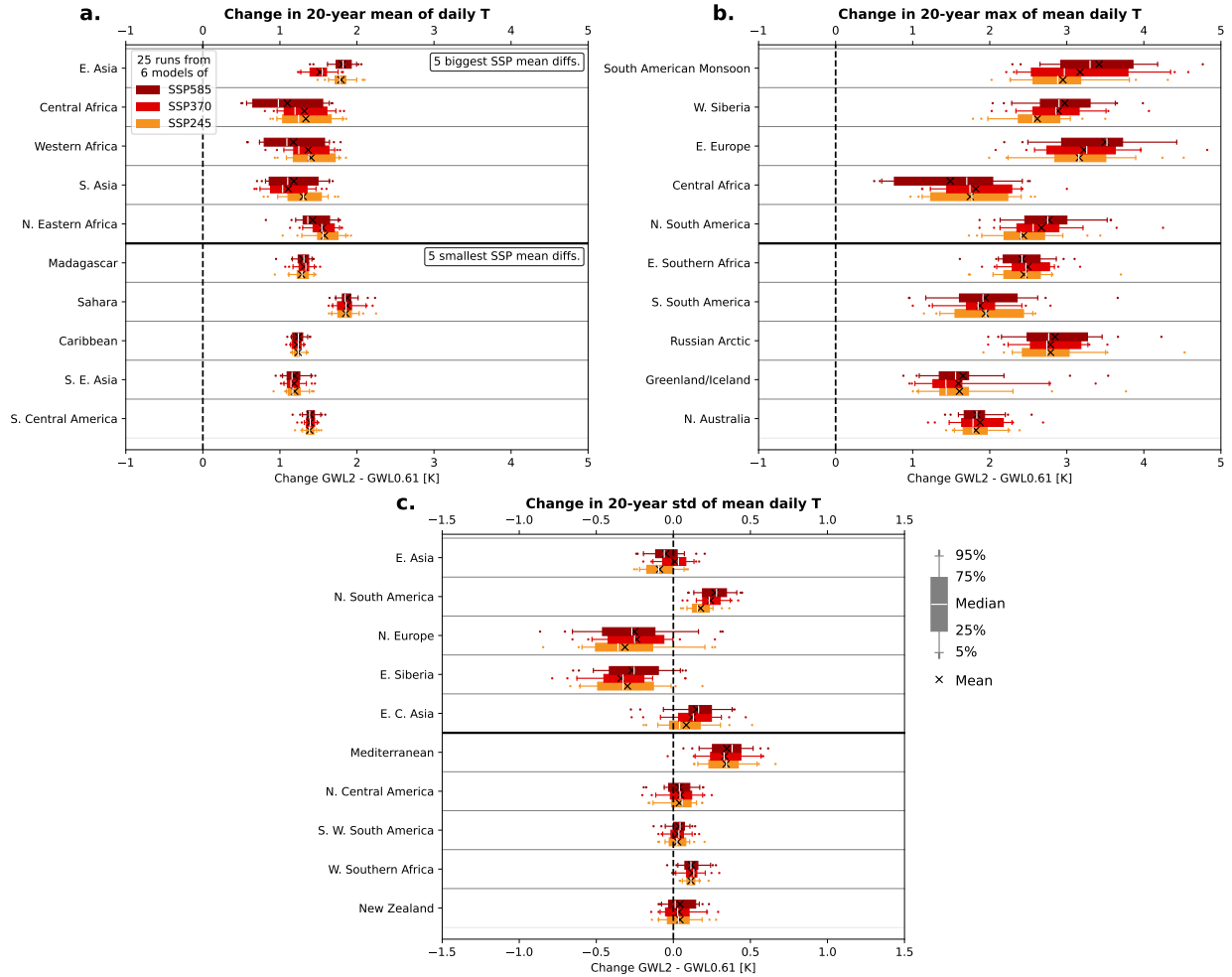


Figure 2: Changes in regionally aggregated statistics for (a.) mean daily temperature (b.) max of daily mean temperature and (c.) standard deviation of daily mean temperature from GWL0.61 to GWL2 by SSP. Each boxplot spans all ESMS and ensemble members. A subset of the BCD-ME is used to ensure the same number of ensemble members are in each sample to allow direct comparisons. All three panels are calculated using the 20 years surrounding each given GWL. The top half of each plot shows the 5 IPCC WG1 regions with the largest differences between SSPs at GWL2, the lower half the regions with the smallest differences.

## 293 4 Technical Validation

### 294 4.1 GWL Assumptions and Validation

295 The primary assumption underlying presenting results by GWL is that local climate conditions are dependent  
 296 only on the amount of warming (represented by GMST) rather than the pathway of warming taken up to  
 297 that point. Two notable ways in which this could affect results across the ScenarioMIP archive is through  
 298 the speed of warming—for instance, the Earth is projected to reach 2.0 °C GWL in 2046 under SSP 2-4.5, but  
 299 an earlier 2038 under the higher emission SSP 5-8.5 (in the BCD-ME, 2036-2055 from the former simulation  
 300 and 2028-2047 from the latter are presented as equivarient simulations at GWL2)—and the dependence on

301 the exact mix of greenhouse gases, aerosols, and other forcings, which may be different at a certain GWL  
302 between SSPs.

303 To confirm that our use of GWL is justified, we show that GWLs are a very good predictor of regional  
304 climate distributions. The distributions in the difference between GWL 2 and the historical GWL 0.61 at the  
305 regional level are indistinguishable between SSPs with no notable bias in mean, variance, or other moments  
306 for a particular SSP (Figure 2). Even SSP3-7.0, which represents a different aerosol trajectory than the other  
307 SSPs<sup>35</sup>, shows a similar distribution of temperature at each GWL to the other scenarios. This analysis was  
308 repeated with other GWLs, with similar results.

## 309 4.2 Physicality of Temperature

310 As a first-pass validation of the final BCD-ME data products, we check for unexpected missing values and  
311 confirm that all temperatures are physically possible. For downscaled statistics, we additionally verify that  
312 average bin-days per year sum up to 365.

## 313 4.3 Validation of QDM bias-correcting method

314 The QDM methodology uses the change in ESM temperature between GWLs and adds it to a reference  
315 bias-corrected model time series. The reference base temperature ESM series is determined using the CDF  
316 of a reanalysis dataset sampled at the quantiles of the ESM ensemble member using 31-day windows around  
317 each day-of-year to define quantiles. The CDF of this reference ESM time series should, thus, be expected  
318 to be nearly identical to the CDF of the reanalysis dataset. Differences between the two CDFs can emerge  
319 from two sources. First, we use 100 quantiles to estimate the true 621-element (31 days x 20 years) empirical  
320 CDF with quantiles between these 100 samples being linearly interpolated. Strong nonlinearities in the  
321 CDF of either the reanalysis dataset or the ESM can, thus, cause discrepancies, as can the interpolation  
322 of extremes. Second, the 30-day rolling window used to estimate quantiles could artificially narrow the  
323 resultant distributions. For example, the rolling window around the hottest day of the year is composed of  
324 that day and 30 colder days.

325 We test the combined influence of these factors on the differences between CDFs of the bias-corrected  
326 ESM at GWL0.61 and the corresponding reanalysis between 1982-2001. We conduct 2-sample Kolmogorov-  
327 Smirnov tests at each grid cell, using a null hypothesis that both the bias-corrected ESM and the reanalysis  
328 CDFs are drawn from the same distribution (Figure 3). Despite the high sensitivity of the Kolmogorov-  
329 Smirnov test to small differences in CDF, low p-values are rare in our analysis. Fewer than 0.1% of grid  
330 cells in the BCD-ME ensemble member with the lowest average p-value have a p-value of less than 0.01, the

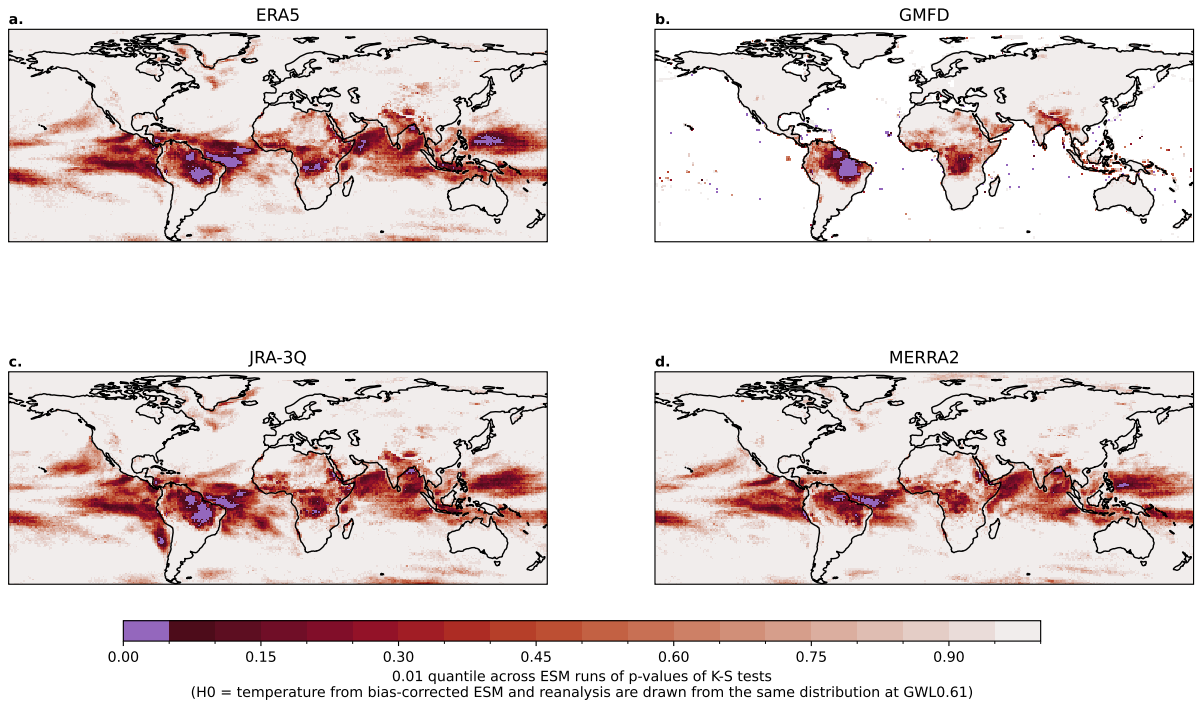


Figure 3: Maps of the 0.01 quantile across BCD-ME ensemble members of p-values of 2-sample Kolmogorov-Smirnov tests at each location against the GWL0.61 daily mean temperature distributions of each reanalysis product and each bias-corrected ensemble member of the BCD-ME being drawn from the same distribution.

331 benchmark significance value used in Cannon et al. (2015)<sup>16</sup>. These low p-values are spatially limited to  
 332 locations over the tropics, particularly over the ocean.

333 In many of the locations with low p-values, the seasonal range of temperature is low and a 31-day rolling  
 334 window captures a large fraction of the total annual temperature range. Thus, the narrowing effect of the  
 335 window would be expected to be most pronounced. Correspondingly, the most anomalous bias-corrected  
 336 CDFs are slightly narrower than their reanalysis counterparts (e.g. Figure 4d). However, any differences in  
 337 the CDF are negligible in practice; in the location with the most differing CDFs in the ensemble member  
 338 with the lowest global average p-value, the largest difference between CDFs is only 0.19 °C (Figure 4d.).

#### 339 4.4 Comparison with NASA NEX-GDDP

340 To verify projected values against previously published work, we compare the BCD-ME to corresponding  
 341 members of the NASA NEX-GDDP dataset<sup>11</sup> which also provides bias-corrected and downscaled daily  
 342 temperature data on a near-global 0.25° grid. The datasets are not exactly comparable – NEX-GDDP  
 343 provides continuous time series instead of chunks organized by GWL, the bias-correction methodologies

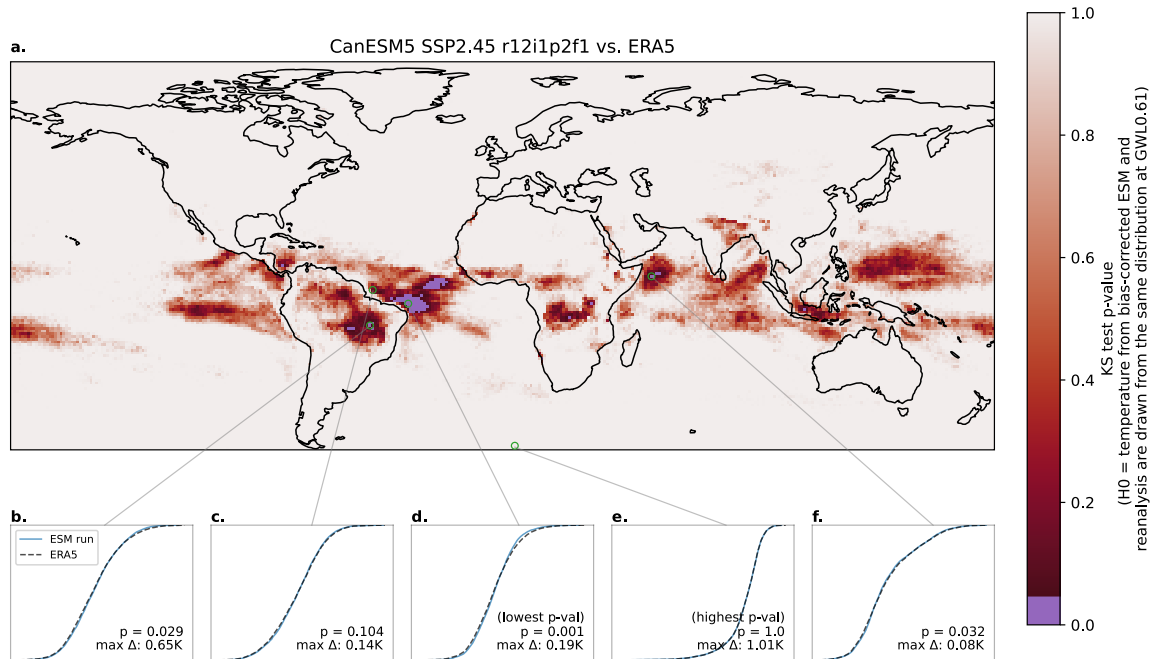


Figure 4: (a.) P-values of 2-sample Kolmogorov-Smirnov tests at each location comparing the ERA5 GWL0.61 daily mean temperature CDF with the CDF of a bias-corrected member from the BCD-ME. We show the r12i1p2f1 from CanESM5 run using SSP2.45, representing the BCD-ME ensemble member with the lowest average p-value, that is, the BCD-ME member for which the CDFs of the ERA5 reference distribution and the bias-corrected ESM are least similar on average. (b.–f.) CDFs of the ESM (blue line) and ERA5 (dashed black line) at various locations, including at the locations with the highest (e.) and lowest (d.) p-values. For each location, we provide the p-value and the maximum temperature difference between the two CDFs at the same quantile.

344 are slightly different, and NEX-GDDP uses 1960-2014 as a reference period instead of the 20 years around  
 345 GWL0.61 used in the BCD-ME. Thus, mean values of temperature are not directly comparable as 1960-2014  
 346 spans a different set of GWLs for each ESM ensemble member.

347 We instead compare *changes* between GWL1.5 and GWL3 for a set of ESMs, experiments, and ensemble  
 348 members common to both the BCD-ME and NEX-GDDP to mitigate these differences in methods (Figure  
 349 5). To best match with NEX-GDDP, we use the the BCD-ME as bias-corrected with GMFD. We determine  
 350 the GWL1.5 and GWL3 20-year periods in NEX-GDDP following our methods in Section 2.2. We expect  
 351 the changes in temperature between GWL1.5 and GWL3 to be similar in NEX-GDDP and the BCD-ME,  
 352 though not identical, for the reasons mentioned above.

353 Differences between mean temperatures at each location are on the order of 0.1 °C with a global mean of  
 354 about 0 in every model run tested (Figure 5). This close alignment of the two products, despite differences  
 355 in methodology, provides evidence that the BCD-ME is an appropriate product for extending analyses  
 356 conducted with NEX-GDDP to account for additional sources of uncertainty.

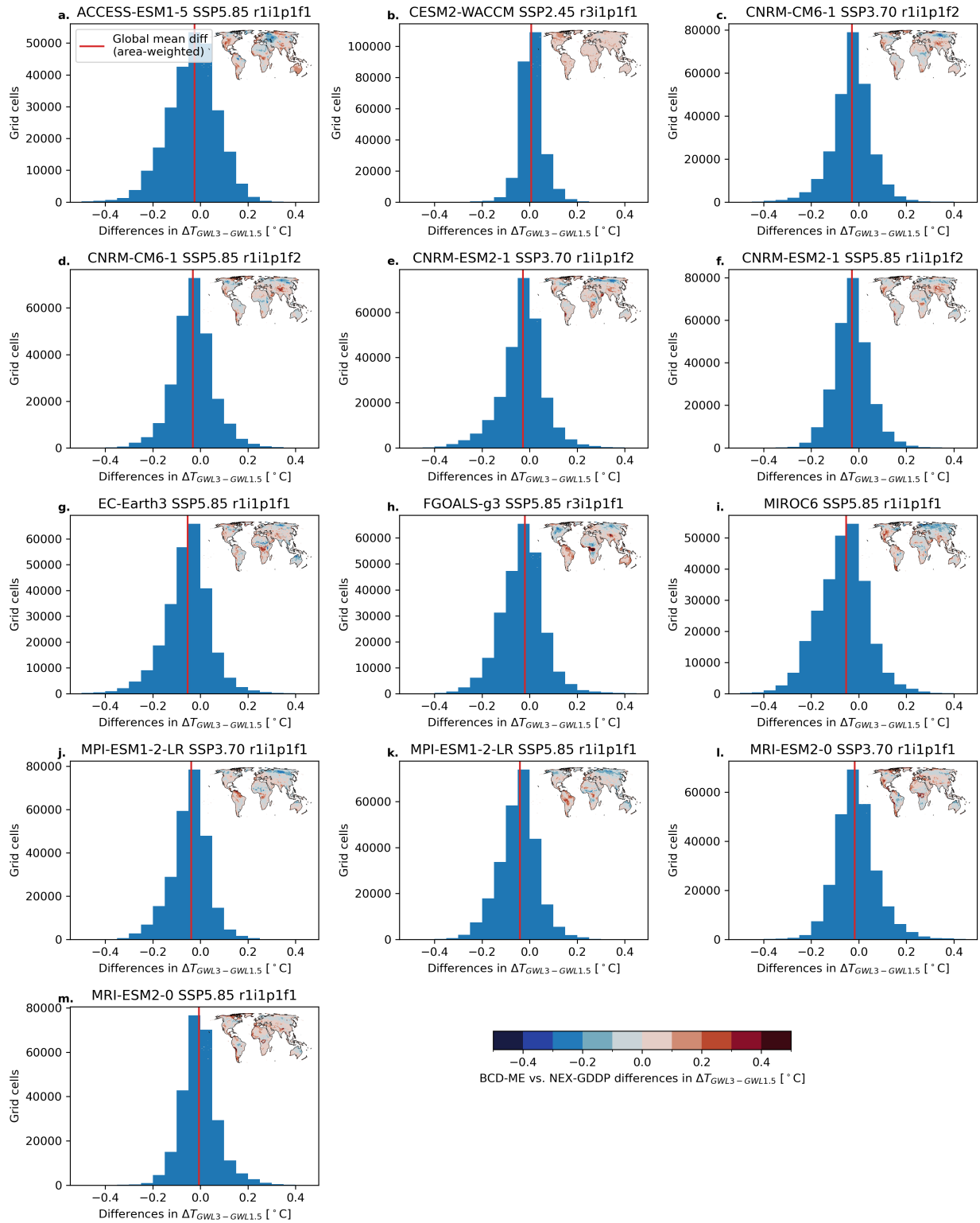
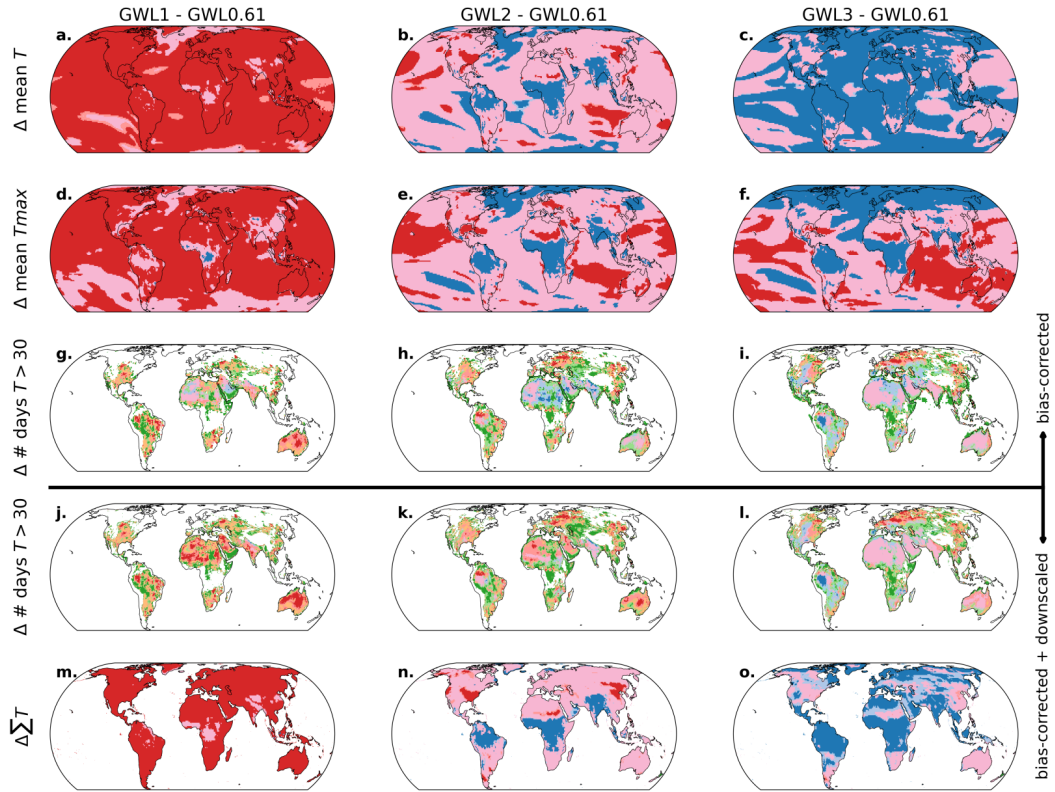


Figure 5: Histograms across grid cells of differences in mean daily temperature between changes from GWL1.5 to GWL3 between corresponding bias-corrected and downscaled ensemble members of the BCD-ME and NASA NEX-GDDP datasets. Inset maps show the spatial distribution of changes.

## 357 4.5 Uncertainty Partitioning Validation

358 The BCD-ME is specifically designed to test the sensitivity of climate impacts projections to three quan-  
359 tifiable sources of climate uncertainty: the irreducible internal variability arising from chaos in the climate  
360 system<sup>6</sup>, the model uncertainty arising from the spread across ESMs outputs driven by the same inputs<sup>7</sup>,  
361 and the observational uncertainty arising from differences between reanalysis estimates of the historical ob-  
362 served climates used to ‘ground truth’ projections<sup>36</sup>. When a researcher utilizes the BCD-ME to propagate  
363 these climate uncertainties to their projections of temperature and related impacts, understanding if the  
364 ultimate uncertainty is primarily due to irreducible uncertainty such as internal variability, or potential re-  
365 ducible uncertainty such as model or observational uncertainty can guide future efforts to better constrain  
366 projections.

367 We thus benchmark the use of the BCD-ME for such partitioning. As such, we calculate the uncertainty  
368 partition of various changes in temperature across bias-corrected and downscaled temperature data (Figure  
369 6). We use the Law of Total Variance to partition the total BCD-ME ensemble variance into internal  
370 variability, model uncertainty, and reanalysis uncertainty. We note that large-scale patterns of uncertainty  
371 partitioning are very similar between the bias-corrected and downscaled projections.



**Partitioning of uncertainty in changes:**

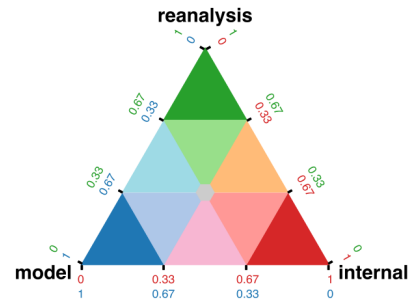


Figure 6: Sample partitioning of uncertainty using the BCD-ME for changes in mean daily temperature (panels a. - c.), maximum daily temperature (d. - f.), number of days / year with mean temperatures above 30 °C (g. - i.), and annual sum of daily temperatures (m. - o.), calculated with up to 12 runs from each ESM for each GWL. Partitioned uncertainty is shown for changes between GWL0.61 (equivalent to 1982-2001 in historical observations) and GWLs 1 (left panel), 2 (middle), and 3 (right panel). The first three rows show results for the bias-corrected set of ensembles, the last two rows show results for the bias-corrected and downscaled set of ensembles.

## 372 5 Usage Notes

373 The BCD-ME data structure is designed with the Python `Xarray` library and is best used in this environment.  
 374 The currently plug-and-play compatibility of `Xarray` with `Zarr` for efficient and fast I/O and with `Dask` for  
 375 parallel computing will provide the highest performance to software development ratio for most users. See  
 376 the provided vignettes in the BCD-ME github repository for introductory examples. For context, the analysis  
 377 used to create Figure 6 required 2.5 hours of computation (45 core-hours) of computation on NSF NCAR’s  
 378 Casper running on all 18 cores of a 2.3-GHz Intel Xeon Gold 6140 (Skylake) CPU with 10 GB RAM/core.  
 379 As much of the computation is embarrassingly parallel, analysis can be expected to roughly scale with the  
 380 number of CPU cores used, provided the system has sufficient I/O.

381 When using the BCD-ME, we recommend users cite both this study as well as the DOI of the BCD-ME  
 382 data archive used to access the data. In addition, we recommend users cite the ESM simulation of any ESM  
 383 used, following the citations provided in Table 4, in addition to the reanalyses used.

Model	Experiment
ACCESS-ESM1-5	SSP2-4.5 <sup>37</sup>
	SSP5-8.5 <sup>38</sup>
CESM2-WACCM	SSP2-4.5 <sup>39</sup>
	SSP3-7.0 <sup>40</sup>
	SSP5-8.5 <sup>41</sup>
CNRM-CM6-1	SSP2-4.5 <sup>42</sup>
	SSP3-7.0 <sup>43</sup>
	SSP5-8.5 <sup>44</sup>
CNRM-ESM2-1	SSP1-1.9 <sup>45</sup>
	SSP1-2.6 <sup>46</sup>
	SSP2-4.5 <sup>47</sup>
	SSP3-7.0 <sup>48</sup>
	SSP4-3.4 <sup>49</sup>
	SSP4-6.0 <sup>50</sup>
	SSP5-3.4-OS <sup>51</sup>
SSP5-8.5 <sup>52</sup>	

Continued on next page

Model	Experiment
CanESM5	SSP2-4.5 <sup>53</sup>
	SSP3-7.0 <sup>54</sup>
	SSP5-8.5 <sup>55</sup>
EC-Earth3	SSP2-4.5 <sup>56</sup>
	SSP3-7.0 <sup>57</sup>
	SSP5-8.5 <sup>58</sup>
EC-Earth3-Veg	SSP2-4.5 <sup>59</sup>
	SSP3-7.0 <sup>60</sup>
	SSP5-8.5 <sup>61</sup>
FGOALS-g3	SSP2-4.5 <sup>62</sup>
	SSP3-7.0 <sup>63</sup>
	SSP5-8.5 <sup>64</sup>
IPSL-CM6A-LR	SSP2-4.5 <sup>65</sup>
	SSP3-7.0 <sup>66</sup>
	SSP5-8.5 <sup>67</sup>
MIROC6	SSP2-4.5 <sup>68</sup>
	SSP3-7.0 <sup>69</sup>
	SSP5-8.5 <sup>70</sup>
MPI-ESM1-2-LR	SSP2-4.5 <sup>71</sup>
	SSP3-7.0 <sup>72</sup>
	SSP5-8.5 <sup>73</sup>
MRI-ESM2-0	SSP2-4.5 <sup>74</sup>
	SSP3-7.0 <sup>75</sup>
	SSP5-8.5 <sup>76</sup>

Table 4: ESM citation information by ESM and scenario, following best practices for citing CMIP simulations.

## 385 **6 Data Availability**

386 The BCD-ME is currently hosted on Arraylake, in the Earthmover Marketplace, in the `s3://ems-climate-uncertainty-lab`  
387 bucket (DOI pending, will be finalized before final publication). This data is freely available under a CC-BY  
388 4.0 license. Sample code to access this data is available as part of the replication code repository on GitHub  
389 under `https://github.com/ks905383/bcd_me/blob/main/code/sample_data_access.ipynb`.

390 By publication, the BCD-ME will also be hosted on the NSF NCAR GEX.

391 Nearly all data needed to replicate the BCD-ME processing can be downloaded entirely using the repli-  
392 cation code below. CMIP6 ESM data was downloaded from the pangeo CMIP6 cloud database. ERA5,  
393 GMFD, and JRA-3Q data was accessed via the NCAR filesystem; this data can alternatively be downloaded  
394 directly from the publishers instead. MERRA-2 data was downloaded from the NASA GES-DISC interface.

## 395 **7 Code Availability**

396 All code required to replicate the BCD-ME and the analysis presented in this Data Descriptor is available at  
397 `https://github.com/ks905383/bcd_me/`; a final static version will be published in a frozen format along  
398 with this paper.

## 399 **8 Author Contributions**

400 Conceptualization: KS

401 Data Curation: KS

402 Formal Analysis: KS, NL

403 Funding Acquisition: KS, NL, RH, GW

404 Investigation: KS

405 Methodology: KS

406 Project Administration: KS

407 Resources: KS, NL

408 Software: KS

409 Supervision: KS, NL, RH, GW

410 Validation: KS, NL

411 Visualization: KS

412 Writing – Original Draft Preparation: NL

413 Writing – Review & Editing: KS, NL, RH, GW

## 414 9 Competing Interests

415 The authors have no known competing interests.

## 416 10 Acknowledgments

417 The authors thank Ryan Abernathy, Tom Bearpark, and Clara Deser for discussion that refined the BCD-ME  
418 analysis. We would like to acknowledge computing support from the Casper system (<https://ncar.pub/casper>)  
419 provided by the NSF National Center for Atmospheric Research (NCAR), sponsored by the National Science  
420 Foundation. We thank Adam Phillips and the NCAR Geoscience Data Exchange (GDEX) team for support  
421 with hosting the BCD-ME. We also thank Earthmover for hosting the living repository of the BCD-ME.

## 422 11 Funding

423 K.S. and R.H. are supported by the National Oceanic and Atmospheric Administration’s Regional Integrated  
424 Sciences and Assessments Program, grant NA21OAR4310313. K.S. is also supported by the Columbia  
425 Climate School Postdoctoral Fellowship Program. N.L. is partially funded through NCAR which is sponsored  
426 by the National Science Foundation under Cooperative Agreement 1852977.

## 427 References

- 428 [1] Eyring, V. *et al.* Overview of the Coupled Model Intercomparison Project Phase 6 (CMIP6) experimental  
429 design and organization. *Geoscientific Model Development* **9**, 1937–1958 (2016).
- 430 [2] Tebaldi, C. & Knutti, R. The use of the multi-model ensemble in probabilistic climate projections.  
431 *Philosophical Transactions of the Royal Society A: Mathematical, Physical and Engineering Sciences*  
432 **365**, 2053–2075 (2007).
- 433 [3] Hawkins, E. & Sutton, R. The Potential to Narrow Uncertainty in Regional Climate Predictions.  
434 *Bulletin of the American Meteorological Society* **90**, 1095–1108 (2009).
- 435 [4] Auffhammer, M., Hsiang, S. M., Schlenker, W. & Sobel, A. Using Weather Data and Climate Model  
436 Output in Economic Analyses of Climate Change. *Review of Environmental Economics and Policy* **7**,  
437 181–198 (2013).
- 438 [5] Rising, J., Tedesco, M., Piontek, F. & Stainforth, D. A. The missing risks of climate change. *Nature*  
439 **610**, 643–651 (2022).

- 440 [6] Schwarzwald, K. & Lenssen, N. The importance of internal climate variability in climate impact pro-  
441 jections. *Proceedings of the National Academy of Sciences* **119**, e2208095119 (2022).
- 442 [7] Burke, M., Dykema, J., Lobell, D. B., Miguel, E. & Satyanath, S. Incorporating Climate Uncertainty  
443 into Estimates of Climate Change Impacts. *The Review of Economics and Statistics* **97**, 461–471 (2015).
- 444 [8] Maraun, D. Bias Correcting Climate Change Simulations - a Critical Review. *Current Climate Change*  
445 *Reports* **2**, 211–220 (2016).
- 446 [9] Schulze, R. Transcending scales of space and time in impact studies of climate and climate change on  
447 agrohydrological responses. *Agriculture, Ecosystems & Environment* **82**, 185–212 (2000).
- 448 [10] Hsiang, S. *et al.* Estimating economic damage from climate change in the United States. *Science* **356**,  
449 1362–1369 (2017).
- 450 [11] Thrasher, B. *et al.* NASA Global Daily Downscaled Projections, CMIP6. *Scientific Data* **9**, 262 (2022).
- 451 [12] Frieler, K. *et al.* Scenario setup and forcing data for impact model evaluation and impact attribu-  
452 tion within the third round of the Inter-Sectoral Impact Model Intercomparison Project (ISIMIP3a).  
453 *Geoscientific Model Development* **17**, 1–51 (2024).
- 454 [13] Gergel, D. R. *et al.* Global Downscaled Projections for Climate Impacts Research (GDPCIR): Preserving  
455 quantile trends for modeling future climate impacts. *Geoscientific Model Development* **17**, 191–227  
456 (2024).
- 457 [14] Hartke, S. H. *et al.* GARD-LENS: A downscaled large ensemble dataset for understanding future climate  
458 and its uncertainties. *Scientific Data* **11**, 1374 (2024).
- 459 [15] Pierce, D. W., Cayan, D. R., Feldman, D. R. & Risser, M. D. Future Increases in North American  
460 Extreme Precipitation in CMIP6 Downscaled with LOCA. *Journal of Hydrometeorology* **24**, 951–975  
461 (2023).
- 462 [16] Cannon, A. J., Sobie, S. R. & Murdock, T. Q. Bias Correction of GCM Precipitation by Quantile  
463 Mapping: How Well Do Methods Preserve Changes in Quantiles and Extremes? *Journal of Climate*  
464 **28**, 6938–6959 (2015).
- 465 [17] Hersbach, H. *et al.* The ERA5 global reanalysis. *Quarterly Journal of the Royal Meteorological Society*  
466 **146**, 1999–2049 (2020).
- 467 [18] Gelaro, R. *et al.* The Modern-Era Retrospective Analysis for Research and Applications, Version 2  
468 (MERRA-2). *Journal of Climate* **30**, 5419–5454 (2017).

- 469 [19] Kosaka, Y. *et al.* The JRA-3Q Reanalysis. *Journal of the Meteorological Society of Japan. Ser. II* **102**,  
470 49–109 (2024).
- 471 [20] Sheffield, J., Goteti, G. & Wood, E. F. Development of a 50-Year High-Resolution Global Dataset of  
472 Meteorological Forcings for Land Surface Modeling. *Journal of Climate* **19**, 3088–3111 (2006).
- 473 [21] Carleton, T. *et al.* Valuing the Global Mortality Consequences of Climate Change Accounting for  
474 Adaptation Costs and Benefits\*. *The Quarterly Journal of Economics* **137**, 2037–2105 (2022).
- 475 [22] Hultgren, A. *et al.* Impacts of climate change on global agriculture accounting for adaptation. *Nature*  
476 **642**, 644–652 (2025).
- 477 [23] Rode, A. *et al.* Estimating a social cost of carbon for global energy consumption. *Nature* **598**, 308–314  
478 (2021).
- 479 [24] Riahi, K. *et al.* The Shared Socioeconomic Pathways and their energy, land use, and greenhouse gas  
480 emissions implications: An overview. *Global Environmental Change* **42**, 153–168 (2017).
- 481 [25] Bosilovich, M. G. *et al.* MERRA-2: Initial Evaluation of the Climate. Tech. Rep. NASA/TM-2015-  
482 104606/Vol.43, NASA (2015).
- 483 [26] Morice, C. P. *et al.* An Updated Assessment of Near-Surface Temperature Change From 1850: The  
484 HadCRUT5 Data Set. *Journal of Geophysical Research: Atmospheres* **126**, e2019JD032361 (2021).
- 485 [27] Lenssen, N. *et al.* A NASA GISTEMPv4 Observational Uncertainty Ensemble. *Journal of Geophysical*  
486 *Research: Atmospheres* **129**, e2023JD040179 (2024).
- 487 [28] Seneviratne, S. I. & Hauser, M. Regional Climate Sensitivity of Climate Extremes in CMIP6 Versus  
488 CMIP5 Multimodel Ensembles. *Earth’s Future* **8**, e2019EF001474 (2020).
- 489 [29] Hausfather, Z., Marvel, K., Schmidt, G. A., Nielsen-Gammon, J. W. & Zelinka, M. Climate simulations:  
490 Recognize the ‘hot model’ problem. *Nature* **605**, 26–29 (2022).
- 491 [30] Milinski, S., Maher, N. & Olonscheck, D. How large does a large ensemble need to be? *Earth System*  
492 *Dynamics* **11**, 885–901 (2020).
- 493 [31] Batibeniz, F., Hauser, M. & Seneviratne, S. I. Countries most exposed to individual and concurrent  
494 extremes and near-permanent extreme conditions at different global warming levels. *Earth System*  
495 *Dynamics* **14**, 485–505 (2023).

- 496 [32] Schlenker, W. & Roberts, M. J. Nonlinear temperature effects indicate severe damages to U.S. crop  
497 yields under climate change. *Proceedings of the National Academy of Sciences* **106**, 15594–15598 (2009).
- 498 [33] Deschênes, O. & Greenstone, M. Climate Change, Mortality, and Adaptation: Evidence from Annual  
499 Fluctuations in Weather in the US. *American Economic Journal: Applied Economics* **3**, 152–185 (2011).
- 500 [34] Abernathy, R. P. *et al.* Cloud-Native Repositories for Big Scientific Data. *Computing in Science &*  
501 *Engineering* **23**, 26–35 (2021).
- 502 [35] Shiogama, H. *et al.* Important distinctiveness of SSP3–7.0 for use in impact assessments. *Nature Climate*  
503 *Change* **13**, 1276–1278 (2023).
- 504 [36] Casanueva, A. *et al.* Testing bias adjustment methods for regional climate change applications under  
505 observational uncertainty and resolution mismatch. *Atmospheric Science Letters* **21**, e978 (2020).
- 506 [37] Ziehn, T. *et al.* CSIRO ACCESS-ESM1.5 model output prepared for CMIP6 ScenarioMIP ssp245  
507 (2019). URL <https://doi.org/10.22033/ESGF/CMIP6.4322>.
- 508 [38] Ziehn, T. *et al.* CSIRO ACCESS-ESM1.5 model output prepared for CMIP6 ScenarioMIP ssp585  
509 (2019). URL <https://doi.org/10.22033/ESGF/CMIP6.4333>.
- 510 [39] Danabasoglu, G. NCAR CESM2-WACCM model output prepared for CMIP6 ScenarioMIP ssp245  
511 (2019). URL <https://doi.org/10.22033/ESGF/CMIP6.10101>.
- 512 [40] Danabasoglu, G. NCAR CESM2-WACCM model output prepared for CMIP6 ScenarioMIP ssp370  
513 (2019). URL <https://doi.org/10.22033/ESGF/CMIP6.10102>.
- 514 [41] Danabasoglu, G. NCAR CESM2-WACCM model output prepared for CMIP6 ScenarioMIP ssp585  
515 (2019). URL <https://doi.org/10.22033/ESGF/CMIP6.10115>.
- 516 [42] Voldoire, A. CNRM-CERFACS CNRM-CM6-1 model output prepared for CMIP6 ScenarioMIP ssp245  
517 (2019). URL <https://doi.org/10.22033/ESGF/CMIP6.4189>.
- 518 [43] Voldoire, A. CNRM-CERFACS CNRM-CM6-1 model output prepared for CMIP6 ScenarioMIP ssp370  
519 (2019). URL <https://doi.org/10.22033/ESGF/CMIP6.4197>.
- 520 [44] Voldoire, A. CNRM-CERFACS CNRM-CM6-1 model output prepared for CMIP6 ScenarioMIP ssp585  
521 (2019). URL <https://doi.org/10.22033/ESGF/CMIP6.4224>.
- 522 [45] Voldoire, A. CNRM-CERFACS CNRM-ESM2-1 model output prepared for CMIP6 ScenarioMIP ssp119  
523 (2019). URL <https://doi.org/10.22033/ESGF/CMIP6.4182>.

- 524 [46] Voldoire, A. CNRM-CERFACS CNRM-ESM2-1 model output prepared for CMIP6 ScenarioMIP ssp126  
525 (2019). URL <https://doi.org/10.22033/ESGF/CMIP6.4186>.
- 526 [47] Voldoire, A. CNRM-CERFACS CNRM-ESM2-1 model output prepared for CMIP6 ScenarioMIP ssp245  
527 (2019). URL <https://doi.org/10.22033/ESGF/CMIP6.4191>.
- 528 [48] Voldoire, A. CNRM-CERFACS CNRM-ESM2-1 model output prepared for CMIP6 ScenarioMIP ssp370  
529 (2019). URL <https://doi.org/10.22033/ESGF/CMIP6.4199>.
- 530 [49] Voldoire, A. CNRM-CERFACS CNRM-ESM2-1 model output prepared for CMIP6 ScenarioMIP ssp434  
531 (2019). URL <https://doi.org/10.22033/ESGF/CMIP6.4213>.
- 532 [50] Voldoire, A. CNRM-CERFACS CNRM-ESM2-1 model output prepared for CMIP6 ScenarioMIP ssp460  
533 (2019). URL <https://doi.org/10.22033/ESGF/CMIP6.4217>.
- 534 [51] Voldoire, A. CNRM-CERFACS CNRM-ESM2-1 model output prepared for CMIP6 ScenarioMIP ssp534-  
535 over (2019). URL <https://doi.org/10.22033/ESGF/CMIP6.4221>.
- 536 [52] Voldoire, A. CNRM-CERFACS CNRM-ESM2-1 model output prepared for CMIP6 ScenarioMIP ssp585  
537 (2019). URL <https://doi.org/10.22033/ESGF/CMIP6.4226>.
- 538 [53] Swart, N. C. *et al.* CCCma CanESM5 model output prepared for CMIP6 ScenarioMIP ssp245 (2019).  
539 URL <https://doi.org/10.22033/ESGF/CMIP6.3685>.
- 540 [54] Swart, N. C. *et al.* CCCma CanESM5 model output prepared for CMIP6 ScenarioMIP ssp370 (2019).  
541 URL <https://doi.org/10.22033/ESGF/CMIP6.3690>.
- 542 [55] Swart, N. C. *et al.* CCCma CanESM5 model output prepared for CMIP6 ScenarioMIP ssp585 (2019).  
543 URL <https://doi.org/10.22033/ESGF/CMIP6.3696>.
- 544 [56] EC-Earth Consortium (EC-Earth). EC-Earth-Consortium EC-Earth3 model output prepared for  
545 CMIP6 ScenarioMIP ssp245 (2019). URL <https://doi.org/10.22033/ESGF/CMIP6.4880>.
- 546 [57] EC-Earth Consortium (EC-Earth). EC-Earth-Consortium EC-Earth3 model output prepared for  
547 CMIP6 ScenarioMIP ssp370 (2019). URL <https://doi.org/10.22033/ESGF/CMIP6.4884>.
- 548 [58] EC-Earth Consortium (EC-Earth). EC-Earth-Consortium EC-Earth3 model output prepared for  
549 CMIP6 ScenarioMIP ssp585 (2019). URL <https://doi.org/10.22033/ESGF/CMIP6.4912>.
- 550 [59] EC-Earth Consortium (EC-Earth). EC-Earth-Consortium EC-Earth3-Veg model output prepared for  
551 CMIP6 ScenarioMIP ssp245 (2019). URL <https://doi.org/10.22033/ESGF/CMIP6.4882>.

- 552 [60] EC-Earth Consortium (EC-Earth). EC-Earth-Consortium EC-Earth3-Veg model output prepared for  
553 CMIP6 ScenarioMIP ssp370 (2019). URL <https://doi.org/10.22033/ESGF/CMIP6.4886>.
- 554 [61] EC-Earth Consortium (EC-Earth). EC-Earth-Consortium EC-Earth3-Veg model output prepared for  
555 CMIP6 ScenarioMIP ssp585 (2019). URL <https://doi.org/10.22033/ESGF/CMIP6.4914>.
- 556 [62] Li, L. CAS FGOALS-g3 model output prepared for CMIP6 ScenarioMIP ssp245 (2019). URL <https://doi.org/10.22033/ESGF/CMIP6.3469>.  
557
- 558 [63] Li, L. CAS FGOALS-g3 model output prepared for CMIP6 ScenarioMIP ssp370 (2019). URL <https://doi.org/10.22033/ESGF/CMIP6.3480>.  
559
- 560 [64] Li, L. CAS FGOALS-g3 model output prepared for CMIP6 ScenarioMIP ssp585 (2019). URL <https://doi.org/10.22033/ESGF/CMIP6.3503>.  
561
- 562 [65] Boucher, O. *et al.* IPSL IPSL-CM6A-LR model output prepared for CMIP6 ScenarioMIP ssp245 (2019).  
563 URL <https://doi.org/10.22033/ESGF/CMIP6.5264>.
- 564 [66] Boucher, O. *et al.* IPSL IPSL-CM6A-LR model output prepared for CMIP6 ScenarioMIP ssp370 (2019).  
565 URL <https://doi.org/10.22033/ESGF/CMIP6.5265>.
- 566 [67] Boucher, O. *et al.* IPSL IPSL-CM6A-LR model output prepared for CMIP6 ScenarioMIP ssp585 (2019).  
567 URL <https://doi.org/10.22033/ESGF/CMIP6.5271>.
- 568 [68] Shiogama, H., Abe, M. & Tatebe, H. MIROC MIROC6 model output prepared for CMIP6 ScenarioMIP  
569 ssp245 (2019). URL <https://doi.org/10.22033/ESGF/CMIP6.5746>.
- 570 [69] Shiogama, H., Abe, M. & Tatebe, H. MIROC MIROC6 model output prepared for CMIP6 ScenarioMIP  
571 ssp370 (2019). URL <https://doi.org/10.22033/ESGF/CMIP6.5752>.
- 572 [70] Shiogama, H., Abe, M. & Tatebe, H. MIROC MIROC6 model output prepared for CMIP6 ScenarioMIP  
573 ssp585 (2019). URL <https://doi.org/10.22033/ESGF/CMIP6.5771>.
- 574 [71] Wieners, K.-H. *et al.* MPI-M MPI-ESM1.2-LR model output prepared for CMIP6 ScenarioMIP ssp245  
575 (2019). URL <https://doi.org/10.22033/ESGF/CMIP6.6693>.
- 576 [72] Wieners, K.-H. *et al.* MPI-M MPI-ESM1.2-LR model output prepared for CMIP6 ScenarioMIP ssp370  
577 (2019). URL <https://doi.org/10.22033/ESGF/CMIP6.6695>.
- 578 [73] Wieners, K.-H. *et al.* MPI-M MPI-ESM1.2-LR model output prepared for CMIP6 ScenarioMIP ssp585  
579 (2019). URL <https://doi.org/10.22033/ESGF/CMIP6.6705>.

- 580 [74] Yukimoto, S. *et al.* MRI MRI-ESM2.0 model output prepared for CMIP6 ScenarioMIP ssp245 (2019).  
581 URL <https://doi.org/10.22033/ESGF/CMIP6.6910>.
- 582 [75] Yukimoto, S. *et al.* MRI MRI-ESM2.0 model output prepared for CMIP6 ScenarioMIP ssp370 (2019).  
583 URL <https://doi.org/10.22033/ESGF/CMIP6.6915>.
- 584 [76] Yukimoto, S. *et al.* MRI MRI-ESM2.0 model output prepared for CMIP6 ScenarioMIP ssp585 (2019).  
585 URL <https://doi.org/10.22033/ESGF/CMIP6.6929>.

## 586 References

- 587 [1] Eyring, V. *et al.* Overview of the Coupled Model Intercomparison Project Phase 6 (CMIP6) experimental  
588 design and organization. *Geoscientific Model Development* **9**, 1937–1958 (2016).
- 589 [2] Tebaldi, C. & Knutti, R. The use of the multi-model ensemble in probabilistic climate projections.  
590 *Philosophical Transactions of the Royal Society A: Mathematical, Physical and Engineering Sciences*  
591 **365**, 2053–2075 (2007).
- 592 [3] Hawkins, E. & Sutton, R. The Potential to Narrow Uncertainty in Regional Climate Predictions.  
593 *Bulletin of the American Meteorological Society* **90**, 1095–1108 (2009).
- 594 [4] Auffhammer, M., Hsiang, S. M., Schlenker, W. & Sobel, A. Using Weather Data and Climate Model  
595 Output in Economic Analyses of Climate Change. *Review of Environmental Economics and Policy* **7**,  
596 181–198 (2013).
- 597 [5] Rising, J., Tedesco, M., Piontek, F. & Stainforth, D. A. The missing risks of climate change. *Nature*  
598 **610**, 643–651 (2022).
- 599 [6] Schwarzwald, K. & Lenssen, N. The importance of internal climate variability in climate impact pro-  
600 jections. *Proceedings of the National Academy of Sciences* **119**, e2208095119 (2022).
- 601 [7] Burke, M., Dykema, J., Lobell, D. B., Miguel, E. & Satyanath, S. Incorporating Climate Uncertainty  
602 into Estimates of Climate Change Impacts. *The Review of Economics and Statistics* **97**, 461–471 (2015).
- 603 [8] Maraun, D. Bias Correcting Climate Change Simulations - a Critical Review. *Current Climate Change*  
604 *Reports* **2**, 211–220 (2016).
- 605 [9] Schulze, R. Transcending scales of space and time in impact studies of climate and climate change on  
606 agrohydrological responses. *Agriculture, Ecosystems & Environment* **82**, 185–212 (2000).

- 607 [10] Hsiang, S. *et al.* Estimating economic damage from climate change in the United States. *Science* **356**,  
608 1362–1369 (2017).
- 609 [11] Thrasher, B. *et al.* NASA Global Daily Downscaled Projections, CMIP6. *Scientific Data* **9**, 262 (2022).
- 610 [12] Frieler, K. *et al.* Scenario setup and forcing data for impact model evaluation and impact attribu-  
611 tion within the third round of the Inter-Sectoral Impact Model Intercomparison Project (ISIMIP3a).  
612 *Geoscientific Model Development* **17**, 1–51 (2024).
- 613 [13] Gergel, D. R. *et al.* Global Downscaled Projections for Climate Impacts Research (GDPCIR): Preserving  
614 quantile trends for modeling future climate impacts. *Geoscientific Model Development* **17**, 191–227  
615 (2024).
- 616 [14] Hartke, S. H. *et al.* GARD-LENS: A downscaled large ensemble dataset for understanding future climate  
617 and its uncertainties. *Scientific Data* **11**, 1374 (2024).
- 618 [15] Pierce, D. W., Cayan, D. R., Feldman, D. R. & Risser, M. D. Future Increases in North American  
619 Extreme Precipitation in CMIP6 Downscaled with LOCA. *Journal of Hydrometeorology* **24**, 951–975  
620 (2023).
- 621 [16] Cannon, A. J., Sobie, S. R. & Murdock, T. Q. Bias Correction of GCM Precipitation by Quantile  
622 Mapping: How Well Do Methods Preserve Changes in Quantiles and Extremes? *Journal of Climate*  
623 **28**, 6938–6959 (2015).
- 624 [17] Hersbach, H. *et al.* The ERA5 global reanalysis. *Quarterly Journal of the Royal Meteorological Society*  
625 **146**, 1999–2049 (2020).
- 626 [18] Gelaro, R. *et al.* The Modern-Era Retrospective Analysis for Research and Applications, Version 2  
627 (MERRA-2). *Journal of Climate* **30**, 5419–5454 (2017).
- 628 [19] Kosaka, Y. *et al.* The JRA-3Q Reanalysis. *Journal of the Meteorological Society of Japan. Ser. II* **102**,  
629 49–109 (2024).
- 630 [20] Sheffield, J., Goteti, G. & Wood, E. F. Development of a 50-Year High-Resolution Global Dataset of  
631 Meteorological Forcings for Land Surface Modeling. *Journal of Climate* **19**, 3088–3111 (2006).
- 632 [21] Carleton, T. *et al.* Valuing the Global Mortality Consequences of Climate Change Accounting for  
633 Adaptation Costs and Benefits\*. *The Quarterly Journal of Economics* **137**, 2037–2105 (2022).
- 634 [22] Hultgren, A. *et al.* Impacts of climate change on global agriculture accounting for adaptation. *Nature*  
635 **642**, 644–652 (2025).

- 636 [23] Rode, A. *et al.* Estimating a social cost of carbon for global energy consumption. *Nature* **598**, 308–314  
637 (2021).
- 638 [24] Riahi, K. *et al.* The Shared Socioeconomic Pathways and their energy, land use, and greenhouse gas  
639 emissions implications: An overview. *Global Environmental Change* **42**, 153–168 (2017).
- 640 [25] Bosilovich, M. G. *et al.* MERRA-2: Initial Evaluation of the Climate. Tech. Rep. NASA/TM-2015-  
641 104606/Vol.43, NASA (2015).
- 642 [26] Morice, C. P. *et al.* An Updated Assessment of Near-Surface Temperature Change From 1850: The  
643 HadCRUT5 Data Set. *Journal of Geophysical Research: Atmospheres* **126**, e2019JD032361 (2021).
- 644 [27] Lenssen, N. *et al.* A NASA GISTEMPv4 Observational Uncertainty Ensemble. *Journal of Geophysical*  
645 *Research: Atmospheres* **129**, e2023JD040179 (2024).
- 646 [28] Seneviratne, S. I. & Hauser, M. Regional Climate Sensitivity of Climate Extremes in CMIP6 Versus  
647 CMIP5 Multimodel Ensembles. *Earth's Future* **8**, e2019EF001474 (2020).
- 648 [29] Hausfather, Z., Marvel, K., Schmidt, G. A., Nielsen-Gammon, J. W. & Zelinka, M. Climate simulations:  
649 Recognize the ‘hot model’ problem. *Nature* **605**, 26–29 (2022).
- 650 [30] Milinski, S., Maher, N. & Olonscheck, D. How large does a large ensemble need to be? *Earth System*  
651 *Dynamics* **11**, 885–901 (2020).
- 652 [31] Batibeniz, F., Hauser, M. & Seneviratne, S. I. Countries most exposed to individual and concurrent  
653 extremes and near-permanent extreme conditions at different global warming levels. *Earth System*  
654 *Dynamics* **14**, 485–505 (2023).
- 655 [32] Schlenker, W. & Roberts, M. J. Nonlinear temperature effects indicate severe damages to U.S. crop  
656 yields under climate change. *Proceedings of the National Academy of Sciences* **106**, 15594–15598 (2009).
- 657 [33] Deschênes, O. & Greenstone, M. Climate Change, Mortality, and Adaptation: Evidence from Annual  
658 Fluctuations in Weather in the US. *American Economic Journal: Applied Economics* **3**, 152–185 (2011).
- 659 [34] Abernathey, R. P. *et al.* Cloud-Native Repositories for Big Scientific Data. *Computing in Science &*  
660 *Engineering* **23**, 26–35 (2021).
- 661 [35] Shiogama, H. *et al.* Important distinctiveness of SSP3–7.0 for use in impact assessments. *Nature Climate*  
662 *Change* **13**, 1276–1278 (2023).

- 663 [36] Casanueva, A. *et al.* Testing bias adjustment methods for regional climate change applications under  
664 observational uncertainty and resolution mismatch. *Atmospheric Science Letters* **21**, e978 (2020).
- 665 [37] Ziehn, T. *et al.* CSIRO ACCESS-ESM1.5 model output prepared for CMIP6 ScenarioMIP ssp245  
666 (2019). URL <https://doi.org/10.22033/ESGF/CMIP6.4322>.
- 667 [38] Ziehn, T. *et al.* CSIRO ACCESS-ESM1.5 model output prepared for CMIP6 ScenarioMIP ssp585  
668 (2019). URL <https://doi.org/10.22033/ESGF/CMIP6.4333>.
- 669 [39] Danabasoglu, G. NCAR CESM2-WACCM model output prepared for CMIP6 ScenarioMIP ssp245  
670 (2019). URL <https://doi.org/10.22033/ESGF/CMIP6.10101>.
- 671 [40] Danabasoglu, G. NCAR CESM2-WACCM model output prepared for CMIP6 ScenarioMIP ssp370  
672 (2019). URL <https://doi.org/10.22033/ESGF/CMIP6.10102>.
- 673 [41] Danabasoglu, G. NCAR CESM2-WACCM model output prepared for CMIP6 ScenarioMIP ssp585  
674 (2019). URL <https://doi.org/10.22033/ESGF/CMIP6.10115>.
- 675 [42] Voldoire, A. CNRM-CERFACS CNRM-CM6-1 model output prepared for CMIP6 ScenarioMIP ssp245  
676 (2019). URL <https://doi.org/10.22033/ESGF/CMIP6.4189>.
- 677 [43] Voldoire, A. CNRM-CERFACS CNRM-CM6-1 model output prepared for CMIP6 ScenarioMIP ssp370  
678 (2019). URL <https://doi.org/10.22033/ESGF/CMIP6.4197>.
- 679 [44] Voldoire, A. CNRM-CERFACS CNRM-CM6-1 model output prepared for CMIP6 ScenarioMIP ssp585  
680 (2019). URL <https://doi.org/10.22033/ESGF/CMIP6.4224>.
- 681 [45] Voldoire, A. CNRM-CERFACS CNRM-ESM2-1 model output prepared for CMIP6 ScenarioMIP ssp119  
682 (2019). URL <https://doi.org/10.22033/ESGF/CMIP6.4182>.
- 683 [46] Voldoire, A. CNRM-CERFACS CNRM-ESM2-1 model output prepared for CMIP6 ScenarioMIP ssp126  
684 (2019). URL <https://doi.org/10.22033/ESGF/CMIP6.4186>.
- 685 [47] Voldoire, A. CNRM-CERFACS CNRM-ESM2-1 model output prepared for CMIP6 ScenarioMIP ssp245  
686 (2019). URL <https://doi.org/10.22033/ESGF/CMIP6.4191>.
- 687 [48] Voldoire, A. CNRM-CERFACS CNRM-ESM2-1 model output prepared for CMIP6 ScenarioMIP ssp370  
688 (2019). URL <https://doi.org/10.22033/ESGF/CMIP6.4199>.
- 689 [49] Voldoire, A. CNRM-CERFACS CNRM-ESM2-1 model output prepared for CMIP6 ScenarioMIP ssp434  
690 (2019). URL <https://doi.org/10.22033/ESGF/CMIP6.4213>.

- 691 [50] Voldoire, A. CNRM-CERFACS CNRM-ESM2-1 model output prepared for CMIP6 ScenarioMIP ssp460  
692 (2019). URL <https://doi.org/10.22033/ESGF/CMIP6.4217>.
- 693 [51] Voldoire, A. CNRM-CERFACS CNRM-ESM2-1 model output prepared for CMIP6 ScenarioMIP ssp534-  
694 over (2019). URL <https://doi.org/10.22033/ESGF/CMIP6.4221>.
- 695 [52] Voldoire, A. CNRM-CERFACS CNRM-ESM2-1 model output prepared for CMIP6 ScenarioMIP ssp585  
696 (2019). URL <https://doi.org/10.22033/ESGF/CMIP6.4226>.
- 697 [53] Swart, N. C. *et al.* CCCma CanESM5 model output prepared for CMIP6 ScenarioMIP ssp245 (2019).  
698 URL <https://doi.org/10.22033/ESGF/CMIP6.3685>.
- 699 [54] Swart, N. C. *et al.* CCCma CanESM5 model output prepared for CMIP6 ScenarioMIP ssp370 (2019).  
700 URL <https://doi.org/10.22033/ESGF/CMIP6.3690>.
- 701 [55] Swart, N. C. *et al.* CCCma CanESM5 model output prepared for CMIP6 ScenarioMIP ssp585 (2019).  
702 URL <https://doi.org/10.22033/ESGF/CMIP6.3696>.
- 703 [56] EC-Earth Consortium (EC-Earth). EC-Earth-Consortium EC-Earth3 model output prepared for  
704 CMIP6 ScenarioMIP ssp245 (2019). URL <https://doi.org/10.22033/ESGF/CMIP6.4880>.
- 705 [57] EC-Earth Consortium (EC-Earth). EC-Earth-Consortium EC-Earth3 model output prepared for  
706 CMIP6 ScenarioMIP ssp370 (2019). URL <https://doi.org/10.22033/ESGF/CMIP6.4884>.
- 707 [58] EC-Earth Consortium (EC-Earth). EC-Earth-Consortium EC-Earth3 model output prepared for  
708 CMIP6 ScenarioMIP ssp585 (2019). URL <https://doi.org/10.22033/ESGF/CMIP6.4912>.
- 709 [59] EC-Earth Consortium (EC-Earth). EC-Earth-Consortium EC-Earth3-Veg model output prepared for  
710 CMIP6 ScenarioMIP ssp245 (2019). URL <https://doi.org/10.22033/ESGF/CMIP6.4882>.
- 711 [60] EC-Earth Consortium (EC-Earth). EC-Earth-Consortium EC-Earth3-Veg model output prepared for  
712 CMIP6 ScenarioMIP ssp370 (2019). URL <https://doi.org/10.22033/ESGF/CMIP6.4886>.
- 713 [61] EC-Earth Consortium (EC-Earth). EC-Earth-Consortium EC-Earth3-Veg model output prepared for  
714 CMIP6 ScenarioMIP ssp585 (2019). URL <https://doi.org/10.22033/ESGF/CMIP6.4914>.
- 715 [62] Li, L. CAS FGOALS-g3 model output prepared for CMIP6 ScenarioMIP ssp245 (2019). URL <https://doi.org/10.22033/ESGF/CMIP6.3469>.
- 716  
717 [63] Li, L. CAS FGOALS-g3 model output prepared for CMIP6 ScenarioMIP ssp370 (2019). URL <https://doi.org/10.22033/ESGF/CMIP6.3480>.
- 718

- 719 [64] Li, L. CAS FGOALS-g3 model output prepared for CMIP6 ScenarioMIP ssp585 (2019). URL <https://doi.org/10.22033/ESGF/CMIP6.3503>.  
720
- 721 [65] Boucher, O. *et al.* IPSL IPSL-CM6A-LR model output prepared for CMIP6 ScenarioMIP ssp245 (2019).  
722 URL <https://doi.org/10.22033/ESGF/CMIP6.5264>.
- 723 [66] Boucher, O. *et al.* IPSL IPSL-CM6A-LR model output prepared for CMIP6 ScenarioMIP ssp370 (2019).  
724 URL <https://doi.org/10.22033/ESGF/CMIP6.5265>.
- 725 [67] Boucher, O. *et al.* IPSL IPSL-CM6A-LR model output prepared for CMIP6 ScenarioMIP ssp585 (2019).  
726 URL <https://doi.org/10.22033/ESGF/CMIP6.5271>.
- 727 [68] Shiogama, H., Abe, M. & Tatebe, H. MIROC MIROC6 model output prepared for CMIP6 ScenarioMIP  
728 ssp245 (2019). URL <https://doi.org/10.22033/ESGF/CMIP6.5746>.
- 729 [69] Shiogama, H., Abe, M. & Tatebe, H. MIROC MIROC6 model output prepared for CMIP6 ScenarioMIP  
730 ssp370 (2019). URL <https://doi.org/10.22033/ESGF/CMIP6.5752>.
- 731 [70] Shiogama, H., Abe, M. & Tatebe, H. MIROC MIROC6 model output prepared for CMIP6 ScenarioMIP  
732 ssp585 (2019). URL <https://doi.org/10.22033/ESGF/CMIP6.5771>.
- 733 [71] Wieners, K.-H. *et al.* MPI-M MPI-ESM1.2-LR model output prepared for CMIP6 ScenarioMIP ssp245  
734 (2019). URL <https://doi.org/10.22033/ESGF/CMIP6.6693>.
- 735 [72] Wieners, K.-H. *et al.* MPI-M MPI-ESM1.2-LR model output prepared for CMIP6 ScenarioMIP ssp370  
736 (2019). URL <https://doi.org/10.22033/ESGF/CMIP6.6695>.
- 737 [73] Wieners, K.-H. *et al.* MPI-M MPI-ESM1.2-LR model output prepared for CMIP6 ScenarioMIP ssp585  
738 (2019). URL <https://doi.org/10.22033/ESGF/CMIP6.6705>.
- 739 [74] Yukimoto, S. *et al.* MRI MRI-ESM2.0 model output prepared for CMIP6 ScenarioMIP ssp245 (2019).  
740 URL <https://doi.org/10.22033/ESGF/CMIP6.6910>.
- 741 [75] Yukimoto, S. *et al.* MRI MRI-ESM2.0 model output prepared for CMIP6 ScenarioMIP ssp370 (2019).  
742 URL <https://doi.org/10.22033/ESGF/CMIP6.6915>.
- 743 [76] Yukimoto, S. *et al.* MRI MRI-ESM2.0 model output prepared for CMIP6 ScenarioMIP ssp585 (2019).  
744 URL <https://doi.org/10.22033/ESGF/CMIP6.6929>.